nzsee
NEW ZEALAND SOCIETY FOR EARTHQUAKE ENGINEERING

Earthquake design loads on retaining walls

J.H. Wood
Retired Civil Engineer, Lower Hutt.

ABSTRACT

Free-standing retaining walls are usually designed for earthquake loads using the Mononobe-Okabe method and assuming cohesionless backfill soil. This simple design approach has led to satisfactory performance and is supported by laboratory testing and analytical studies. For major wall structures there are a number of refinements to the method that should be considered. In the paper methods of assessing the influence on the earthquake loads of the flexibility of the wall, soil cohesion and ground water in the backfill are presented. Methods for predicting failure plane angles to allow a better assessment of the soil properties within the failure wedge are presented. Procedures for estimating the outward displacement and the influence of passive resistance and wall geometry on the sliding resistance are discussed. Design charts are presented which allow the magnitude of these refinements to be rapidly assessed.

1 INTRODUCTION

It is usual to simplify the complex problem of the interaction of earthquake generated elastic waves in the soil with wall structures by assuming that the earthquake ground motions are equivalent to dynamic inertia forces acting in the backfill mass. Dynamic pressures on the wall can then be estimated by analysing the wall and backfill modelled as an elastic continuum or failure wedge in the soil subjected to both gravity and horizontal and vertical inertia forces. The pressures that develop are very sensitive to the elastic flexibility of the structural and foundation components of the wall, and the ability of the wall to move outward (rotation or translation) because of either permanent deformation in the foundation soils or inelastic behaviour of the structure.

The behaviour of wall structures during earthquakes can be broadly classified into three categories related to the maximum strain condition that develops in the soil near the wall. The soil may remain essentially elastic, respond in a significantly nonlinear manner, or become fully plastic. The rigidity of the wall and its foundations will have a strong influence on the type of soil condition that develops.

Many low walls are of cantilever type construction. In this type of wall, lateral pressures from vertical gravity and earthquake forces will often produce sufficient displacement within the wall structure and foundation to induce a fully plastic stress state in the retained soil. In more rigid free-standing walls, such as gravity (e.g. mechanically stabilised earth and concrete block walls) counterfort walls and building basement walls, a fully plastic stress state may develop as the result of permanent outward movement from sliding or

rotational deformations in the foundation. In cases where significant nonlinear soil behaviour or a fully plastic stress state occurs in the backfill soil during earthquake loading, the well-known Mononobe-Okabe, (MO) method (Mononobe and Matsuo 1929) can be used to compute earthquake pressures and forces acting on the wall.

Retaining structures that are not free-standing or have rigid foundations (piles or footings on rock or stiff soil) may not displace sufficiently, even under severe earthquake loading, for a fully plastic stress state to develop in the soil backfill. For these types of walls, it is important to estimate the displacements to check the applicability of the MO method. It is more difficult to analyse these stiff walls but the earthquake loads can be satisfactorily estimated by interpolation between loads based on elastic rigid wall and MO theory.

2 WALL FLEXIBILITY

2.1 Flexibility Parameters

The author (Wood 2019) carried out elastic finite element analyses on cantilever walls that deform by both rotation about their base and flexure in the wall stem. The wall stiffness parameters were varied to produce pressure distributions under horizontal earthquake and gravity loads for walls that vary from rigid to sufficiently flexible for the MO method to be applicable. Tension pressures acting normal to the wall were eliminated. Both smooth and bonded soil-wall contacts were considered and backfill soils with a shear modulus both uniform over the height and with a linear increase from zero at the top of the wall to a maximum at the base were used. Rectangular plain strain elements were used to model the soil, and beam elements to model the wall.

Results for the walls deforming in flexure were presented in terms of a flexibility parameter d_w defined by:

$$d_w = \frac{G\,H^3}{E_w I_w} \qquad (1)$$

Where G is the average soil shear modulus, H the height of the retained soil layer, E_w is the Young's modulus for the wall material and I_w the second moment of area of the wall per unit length.

Results for the walls deforming by rotation about the base were presented in terms of a flexibility parameter d_θ defined by:

$$d_\theta = \frac{G\,H^2}{R_\theta} \qquad (2)$$

Where R_θ is the rotational stiffness of the wall footing per unit length.

2.2 Pressure distributions

Pressure distributions acting on the walls are presented in Wood 2019. For a given flexibility ratio d_w or d_θ, the normal pressures acting on the wall are dependent on the acceleration coefficient C_o, soil unit weight γ, and the height of the retained soil H, but are independent of the soil stiffness parameter directly. The total force acting on the wall, V_b (or shear force at the base of the stem) and the bending moment at the base of the wall stem, M_b were obtained by integrating the pressure distributions.

2.3 Shears and Moments

Shears and moments per unit length for flexural deformation of the wall and the corresponding force actions for the wall deforming by base rotation are shown in Figures 1 and 2, and 3 and 4 respectively.

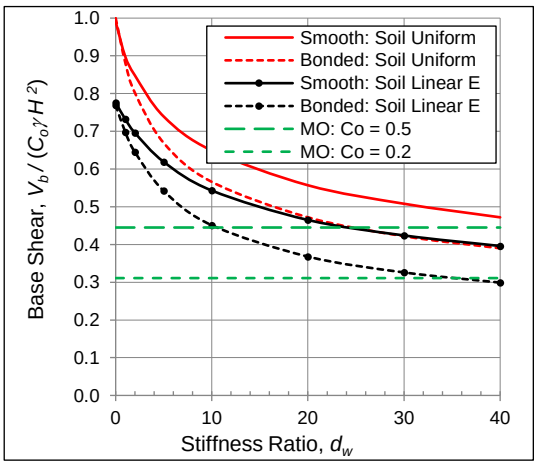

Figure 1. Base shear for flexure deformation.

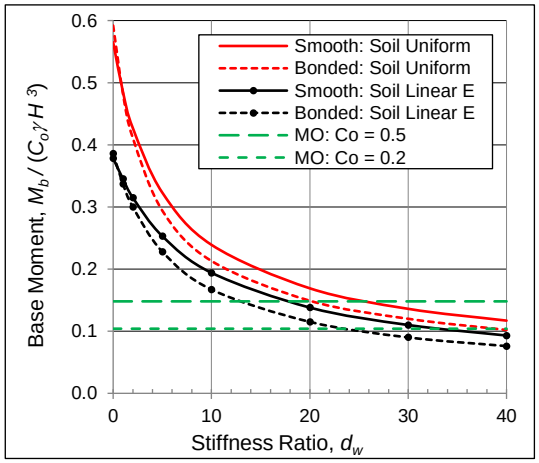

Figure 2. Base moment for flexure deformation.

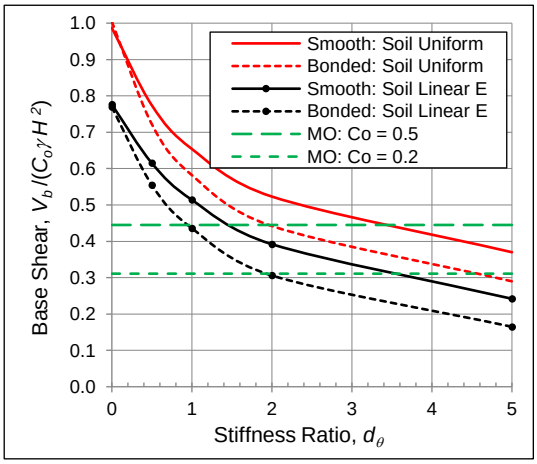

Figure 3. Base shear for rotational deformation.

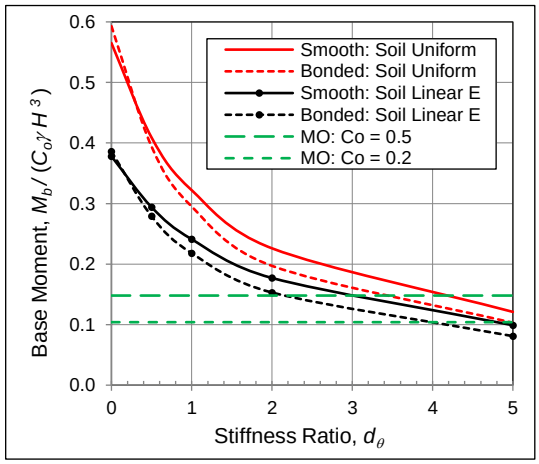

Figure 4. Base moment for rotational deformation.

The shears and moments shown in Figures 1 to 4 are plotted in dimensionless terms so that they can be used to evaluate solutions for any values of C_o, γ and H. A Poisson's ratio of 0.33 was assumed for the soil.

Superimposed on the plots are MO forces and moments calculated for a smooth wall assuming a soil friction angle $\phi = 35°$. MO values are plotted for acceleration coefficient values of $C_o = 0.2$ and 0.5. Since the MO actions do not vary linearly with C_o and are independent of d_w and d_θ, they are drawn as separate horizontal lines for typical C_o values used in design.

The shears and moments shown in Figures 1 to 4 do not include the components from gravity load in the backfill. Gravity pressures for rigid walls can be calculated using the at-rest assumption ($K_o = 1 - \sin\phi$) and for flexible walls Rankine active pressure can be assumed. Gravity pressures for intermediate or stiff walls, and deflections predicted by elastic finite element analyses are given in Wood (2019).

3 GENERALISED MONONOBE-OKABE

3.1 Analysis Method

Shukla (2015) presented a generalised analytical expression in explicit form for the pseudo-static earthquake active thrust from c–ϕ soil backfills on a rigid retaining wall. The expression is an extension of the MO equation for cohesionless soil and as for the MO analysis method assumes that sufficient outward movement of the wall occurs (translation or rotation) for active pressures to develop. The generalised analysis considers, inclination of the wall-soil interface, backfill slope angle, surcharge on the backfill, tension cracks,

wall-backfill friction and adhesion, cohesion and angle of shearing resistance of the backfill, and both horizontal and vertical earthquake accelerations. An explicit analytical expression for the critical inclination of the failure plane within the soil backfill is also presented. Figure 5 from Shukla shows the definition diagram for the generalised analysis.

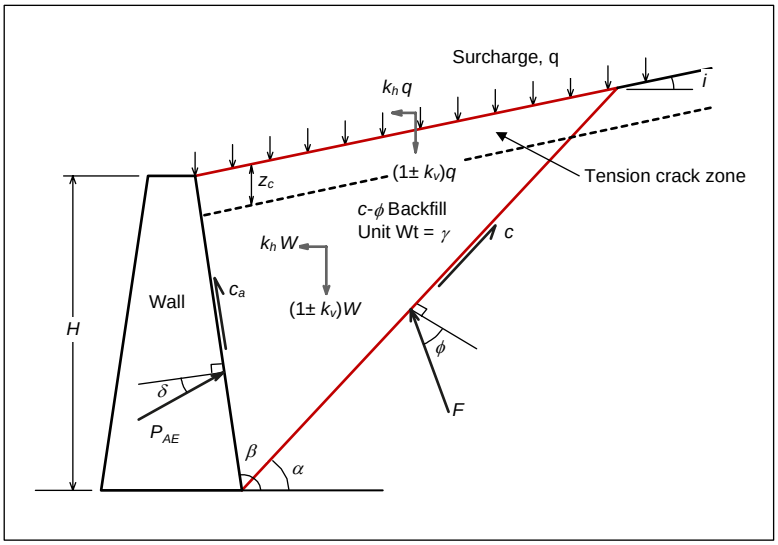

Figure 5. Forces acting on failure wedge for c-ϕ soil and generalised field conditions. From Shukla (2015).

Shukla (2013) published the equivalent solution for passive pressure with the wall forced against the backfill and the horizontal inertia force acting on the soil wedge in the opposite direction to that shown in Figure 5. (See Section 6.3 below.)

3.2 Active Pressure Force

The active earthquake pressure force P_{AE} on the back face of the wall from the failure wedge (including the gravity component) is given by:

$$P_{AE} = 0.5K_{AE}\,\gamma H^2 \tag{3}$$

$$K_{AE} = (1 \pm k_v)\left[\frac{2q}{\gamma H} + \frac{\sin(\beta - i)}{\sin(\beta)}\right] K_{AE\gamma} \mp \frac{c}{\gamma H}\left[2 - \frac{z_c}{H}\right] K_{AEc} \tag{4}$$

$$K_{AE\gamma} = \frac{\sin(\beta - \alpha_c)\sin(\pm\theta \mp \emptyset + \alpha_c)}{\cos\theta\, sin\beta\, \sin(\alpha_c - i)\, \sin(\beta \pm \delta \pm \emptyset - \alpha_c)} \tag{5}$$

$$K_{AEc} = \frac{a_f\, \cos(\beta \pm \emptyset - \alpha_c) + \frac{\sin(\beta - i)cos\emptyset}{\sin(\alpha_c - i)}}{sin\beta\, \sin(\beta \pm \delta \pm \emptyset - \alpha_c)} \tag{6}$$

Where q is the vertical surcharge on the backfill surface, c the soil cohesion on the failure plane, c_a the adhesion on the wall-backfill interface, a_f the adhesion factor = c_a/c, z_c the tension crack depth, ϕ the peak soil friction angle, β the wall inclination (positive in an anticlockwise direction from the horizontal), δ the friction angle on the wall-soil interface, i the soil backslope angle (from horizontal), α_c the critical failure plane angle and θ the seismic inertia angle given by:

$$\theta = tan^{-1}\left[\frac{k_h}{1 \pm k_v}\right] \tag{7}$$

Where k_h is the horizontal acceleration coefficient and k_v is the vertical acceleration coefficient.

Equations 3 to 7 can be used for the passive pressure case by applying the lower of the signs where both + and – signs are indicated. In the passive case z_c is assumed to be zero.

The angle parameters and the forces acting on the failure wedge in the backfill are shown in Figure 5. Based on Rankine's analysis the tension crack depth can be taken as (Terzaghi et al 1996):

$$z_c = \frac{2c}{\gamma} tan\left(\frac{\pi}{4} + \frac{\emptyset}{2}\right) \quad (8)$$

Equations 5 and 6 for $K_{AE\gamma}$ and K_{AEc} are in expressed in terms of the critical failure plane angle α_c. Shukla (2015) gives closed form expressions for α_c but they are too complicated to present here. The critical angle can be determined by iteration to find the maximum value of K_{AE} (Equation 4). The Excel Solver add-in is a convenient method of undertaking this iteration directly and is a more straightforward method for calculating α_c than evaluating the closed form equations.

K_{AE} and α_c versus the cohesion factor $2c/\gamma H$ are plotted for a backfill with $\phi = 30°$ in Figures 6 and 7 respectively. Similar plots for a backfill friction angle of 35° are shown in Figures 8 and 9 respectively. Curves are shown for k_h values of 0.1, 0.2 and 0.3 and for each k_h value a backfill surface inclination curve is shown for i values of 0°, 10° and 20°. To calculate the results shown in Figures 6 to 9 it was assumed that z_c was as given by Equation 8, $\beta = 90°$, $\delta = 2/3\phi$, $a_f = 0.5$ and k_v and $q = 0$. The force on the wall P_{AE} is calculated from K_{AE} using Equation 3 and is orientated at an angle δ to the normal to the wall as shown in Figure 5. Figures 6 and 8 show that small amounts of cohesion reduce the K_{AE} values significantly.

It is important to estimate the failure plane angle for the backfill soil and consider the influence of the surrounding soil outside the limits of the backfill zone. When the failure plane angle is predetermined by the boundary between the backfill and a surrounding soil with significantly greater shear strength than the backfill, K_{AE} can be calculated using the predetermined angle in Equations 5 and 6 rather than α_c. This situation may arise where the soil outside the backfill zone has significant cohesion or is rock.

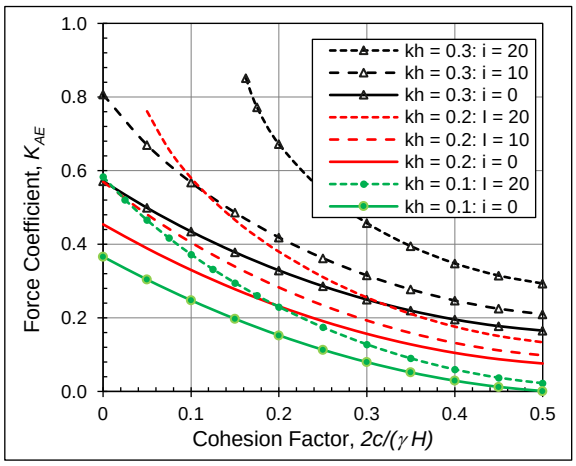

Figure 6. Force coefficient for $\phi = 30°$.

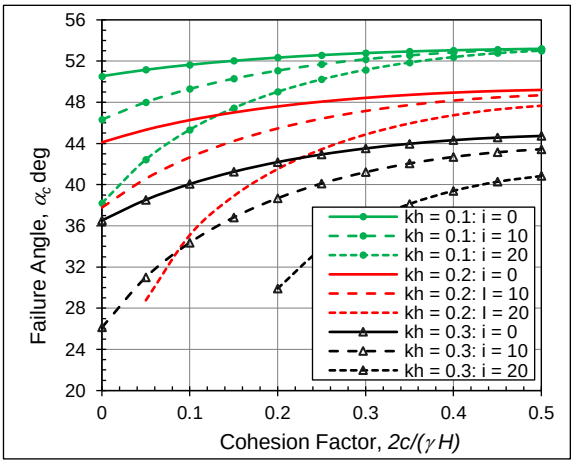

Figure 7. Failure plane angle for $\phi = 30°$.

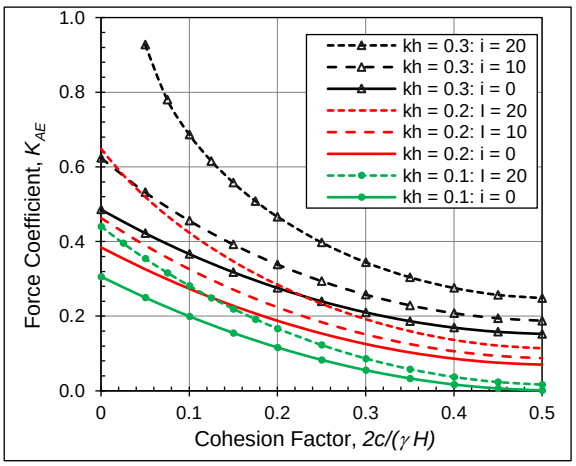

Figure 8. Force coefficient for $\phi = 35°$.

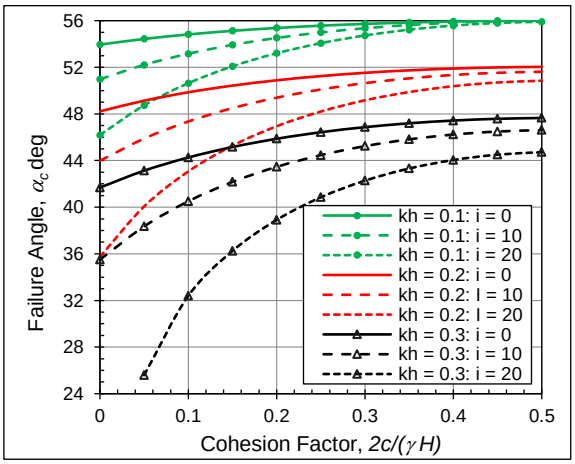

Figure 9. Failure plane angle for $\phi = 35°$.

4 OUTWARD DISPLACEMENT

For high earthquake acceleration coefficients and walls with steep backfill slopes it will often be advantageous to design for permanent displacements arising from sliding and rotation of the wall, soil foundation deformation or ductility in the wall structure. The design can then be based on the critical acceleration to initiate permanent displacement rather than the peak ground acceleration (PGA).

The outward movement of walls resulting from sliding, foundation bearing failures, or a ductile failure in the wall structure can be estimated using the Newmark Sliding Block theory (Wood 2008). Outward movement can be conveniently estimated using the Jibson (2007) correlation equation. This was derived by statistical analysis of the displacements calculated from numerical sliding block computations using 2,270 strong motion acceleration records. The Jibson equation for the mean permanent outward displacement, *d* expressed in centimetres is given by:

$$\log(d) = -0.271 + log\left[\left(1 - \frac{a_c}{a_{max}}\right)^{2.335}\left(\frac{a_c}{a_{max}}\right)^{-1.478}\right] + 0.424M_w \qquad (9)$$

Where a_c is the critical acceleration to initiate sliding failure, a_{max} is the PGA in the acceleration record, and M_w the earthquake moment magnitude. The displacement is normally distributed with a standard deviation of 0.454. Evaluation of Equation 9 requires the calculation of the a_c/a_{max} ratio, selection of an appropriate earthquake magnitude and deciding on an appropriate level for the probability of exceedance of the calculated displacement using the standard deviation.

A displacement versus a_c/a_{max} curve from the evaluation of Equation 9 for M_w = 7.0 and a 16% probability of exceedance is compared with four other displacement correlation equations in Figure 10. (The other correlation equations are given in the referenced papers in the figure legend.)

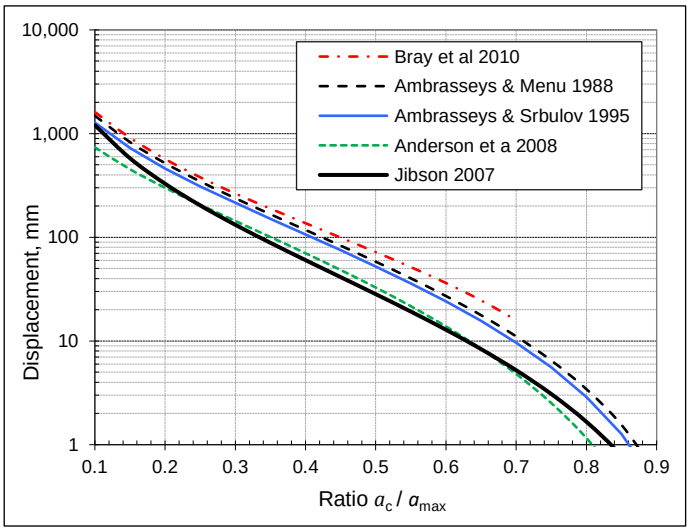

Figure10 shows that for a critical acceleration of one-half of the PGA the permanent outward movement of the sliding mass in a M_w 7.0 earthquake is likely to be in the range of 30 to 70 mm (16% probability of exceedance). Many wall structures would not be seriously damaged by movements of this order.

Some rotation of a wall structure may occur when the wall slides outward and it is therefore likely that the displacements at the top of the wall could be up to 50% higher than estimated from the rigid siding block assumption.

Figure 10. Displacements from Jibson (2007), and other correlation equations.

5 SUBMERGED BACKFILL SOIL

Matsuzawa et al (1985) developed a method for calculating lateral earthquake pressures against a rigid wall from soil and water when the backfill soil is submerged. The method is based on the MO analysis procedure for unsaturated backfill soil.

5.1 Highly Permeable Backfill

For highly permeable soils Matsuzawa et al (1985) assumed that the pore water can move freely in the voids without restriction from the soil particles. The vertical body force during the earthquake can be calculated by

subtracting the dynamic buoyancy force acting on the solid particles from the total dynamic force. Therefore, the apparent seismic inertia angle θ' can be calculated by:

$$tan\theta' = \frac{F_H}{F_V} = \left(\frac{G_s}{G_s - 1}\right)\left(\frac{k_h}{1 \pm k_v}\right) = \frac{G_s}{G_s - 1} tan\theta \quad (12)$$

Where G_s is the specific gravity of the soil particles. For most soils G_s is approximately 2.6 so the effective seismic coefficient is about 1.6 times the true seismic coefficient for an unsaturated backfill soil.

For a highly permeable soil a dynamic water pressure needs to be added to the pressure from the soil particles. Westergaard (1933) proposed the following approximate solution for the water pressure force on a vertical wall with a semi-infinite long water reservoir:

$$P_{wd} = \frac{7}{12} k_h \gamma_w H_w^2 \quad (13)$$

Where γ_w is the unit weight of water having a height of H_w above the wall base. The water pressure force acts at a height 0.4 H above the base of the wall. The water flow will usually be restricted by the soil particles and boundaries so Equation 13 will give a conservative estimate of the water force.

5.2 Low Permeability Backfill

For low permeability backfills Matsuzawa et al (1985) assumed that the solid portion and the pore water portion of the soil element behave as a unit. Therefore, the total unit weight of the soil is subjected to the horizontal acceleration and thus the horizontal inertia body force, F_H is equal to $\gamma_{sat} k_h$. The apparent inertia angle of the seismic coefficient becomes:

$$tan\theta'' = \frac{F_H}{F_V} = \frac{\gamma_{sat}}{\gamma_{sub}}\left(\frac{k_h}{1 \pm k_v}\right) = \frac{\gamma_{sat}}{\gamma_{sat} - \gamma_w}\left(\frac{k_h}{1 \pm k_v}\right) tan\theta \quad (14)$$

Where γ_{sat} and γ_{sub} are the saturated and submerged unit weight of the soil respectively.
The saturated unit weight of soil is approximately two times the unit weight of water giving an effective horizontal seismic coefficient of approximately two times the value for unsaturated soil.

5.3 Comparison of Forces from High and Low Permeability Backfill

Figure 11 shows a comparison of the dimensionless horizontal force, P_{AEd} $[(P_{AE}/(0.5\gamma_{bulk} H^2)]$ acting on a rigid wall for an unsaturated backfill soil, with saturated backfill having both high and low permeability over the range of k_h values used in design. The bulk unit weight of the soil, γ_{bulk} was assumed to be 18 kN/m^3, the saturated unit weight 19.5 kN/m^3 and the soil specific gravity 2.65. The soil friction angle, ϕ was assumed to be 35° (cohesionless soil) with the friction angle on the wall-soil interface taken as 2/3ϕ.

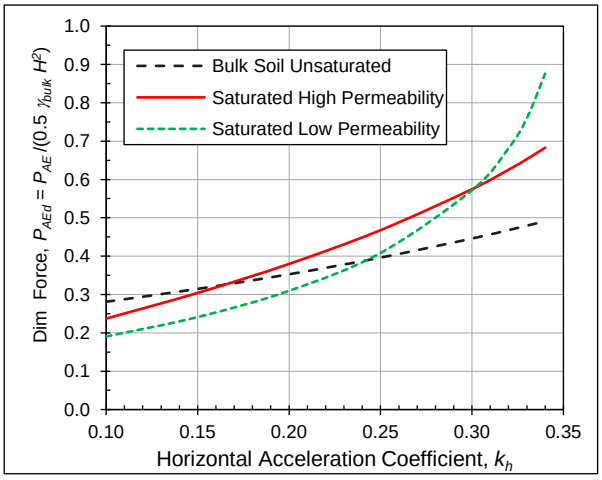

Over the k_h range of interest for low walls – 0.15 to 0.25 - there is only a small difference between the force from unsaturated (based on bulk density) and the force from saturated high permeability soil (including the dynamic water force). Matsuzawa et al (1985) developed a generalised apparent inertia angle to cover a wide range of backfill types with intermediate permeabilities but for wall design Figure 13 shows that for k_h values less than 0.3 assuming a high permeability soil gives a moderately conservative result for all permeabilities.

Figure 11. Earthquake forces from unsaturated and saturated soils.

5.4 Partially Submerged Backfill

For the case when the water level is below the top of the wall Kramer (1996) suggested that the earthquake soil thrust on the wall could be computed using an average unit weight based on the relative volumes of soil within the active wedge that are above and below the phreatic surface (γ_{bulk} above water and γ_{sub} below). Hydrostatic and hydrodynamic (if any) thrusts must be added to the soil thrust.

6 SLIDING RESISTANCE AND PASSIVE PRESSURES

6.1 Cohesionless Foundation Soil

The sliding resistance of cantilever and gravity walls is usually taken as the sum of the friction force on the base of the footing and the passive resistance on the effective toe depth of the wall. Figure 12 shows the failure slip lines calculated using LimitState: GEO (Smith and Cubrinovski 2011) for a 2.5 m high cantilever wall subjected to gravity, live load (4 kPa) and horizontal earthquake loads. Both the backfill and foundation soil were assumed to be cohesionless with a friction angle of 30°. All soil-wall interfaces were set to a friction coefficient of 0.5 tanϕ = 0.29. The critical acceleration to initiate sliding displacement was 0.23 g. The slip lines indicate that the 0.2 m deep key at the rear of the footing has a significant influence on sliding resistance and suggest that the depth to be used in estimating the passive resistance should be taken as at least the sum of the footing and key depth. The key also initiates failure through the soil rather than on the interface of the soil with the footing base.

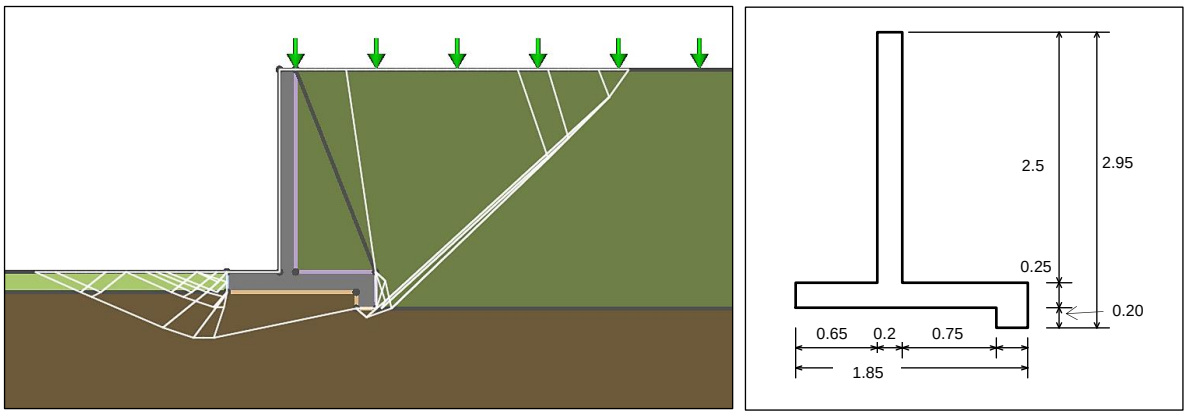

Figure 12. Failure slip lines for cantilever wall.

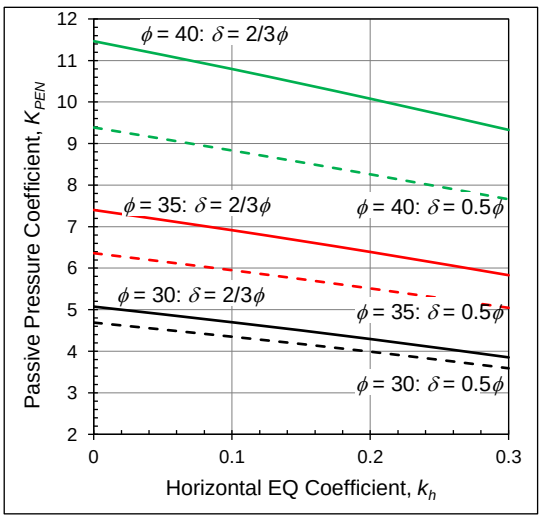

Figure 13. Passive pressure coefficient for cohesionless soil.

Numerical results for the passive resistance of a cohesionless soil-wall interface under earthquake loading have been presented by Choudhury (2004), Kumar (2001), Morrison and Ebeling (1995), Mylonakis et al (2007), Soubra (2000) and Subba Rao & Choudhury (2005). The MO equation can be used to calculate the passive resistance (with sign changes from the active case) but significantly overestimates the resistance for friction angles greater than 30° and when there is significant soil-wall interface friction.

Results from Soubra for the earthquake force passive pressure coefficient on a vertical wall with a horizontal ground surface are shown in Figure 13 for soil friction values of ϕ equal to 30°, 35° and 40°.

Pressure coefficients for two soil-wall interface friction values of 0.5ϕ and $2/3\phi$ are shown for each of the soil friction values. The passive pressure coefficient K_{PEN} is for the force component normal to the wall. Soubra used a translational multiblock failure mechanism which is essentially a generalisation of the single block used in the MO analysis method. A comparison of the Soubra pressure coefficients with the results from the other researchers listed above showed good agreement.

6.2 Cohesive Foundation Soil

For purely cohesive soils the Shukla 2013 generalised analytical expressions given in Equations 3 to 7 above can be used to estimate the passive pressure acting on a soil-wall interface. For a vertical wall face with a horizontal ground surface these expressions can be greatly simplified. Assuming a plane failure surface the dimensionless passive pressure force normal to the wall is given by:

$$P_{PED} = \frac{P_{PE}}{0.5\gamma H^2} = (cosec\alpha_c \, sec\alpha_c)\frac{2c}{\gamma H} + (1 - k_h cot\alpha_c) \qquad (15)$$

The critical failure plane angle from the horizontal is given by:

$$\alpha_c = Atan\sqrt{\frac{1-\frac{k_h\gamma H}{2c}}{1+a_f}} \qquad (16)$$

A plot of the dimensionless passive pressure force P_{PED} versus the cohesion factor, $2c/(\gamma H)$ is shown in Figure 14 for k_h values of 0, 0.1, 0.2, 0.3 and 0.4. The a_f value (adhesion on the soil-wall interface) was taken as 0.5. Except for low cohesion factors the pressure force varies almost linearly with this ratio.

6.3 *c-ϕ* Foundation Soils

For soils with both cohesion and friction the solutions of Soubra (2000) and Shukla (2013) can be applied but both have limitations. For friction angles greater than 30° and high soil-wall interface friction the plane failure surface assumption of Shukla results in an overestimation of the passive force. Soubra's (2000) numerical results are only tabulated for friction angles greater than 15° but provided the friction angle is greater than this value these results give values suitable for design. An acceptable approach for design when the backfill friction angle is greater than 30° would be to add the friction component shown in Figure 13 to the cohesion component shown in Figure 14. For friction angles less than 30° the Shukla (2013) equations can be used and should give acceptable force predictions although possibly too high by a small amount. (Reference can be made to the Soubra (2000) results for ϕ down to 15°).

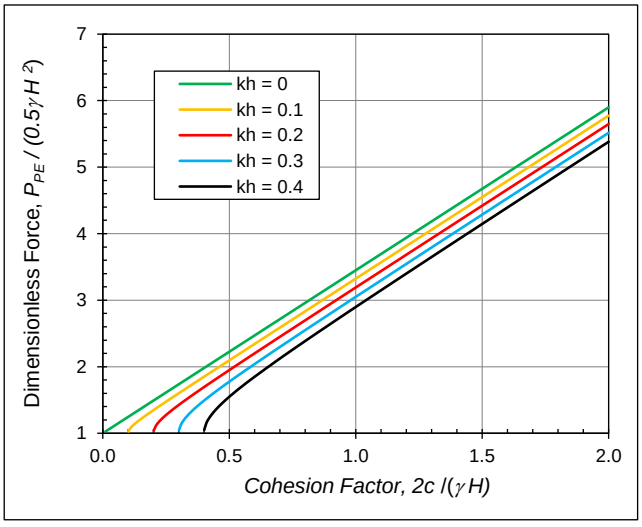

Figure 14. Passive pressure force for cohesive soil

6.4 Location of Shear Key

The location of the shear key has a major influence on the sliding resistance under both gravity and earthquake load cases for a cohesionless foundation soil but has little influence for an undrained cohesive foundation soil. An analysis of the cantilever wall shown in Figure 12 using LimitState:GEO and the cohesionless soil described in Section 6.1 with the key located at the front of the footing, under the stem and at the rear of the footing gave critical accelerations to initiate sliding of 0.07g, 0.15 g and 0.23 g respectively.

7 CONCLUSIONS

The elastic flexibility of the wall and wall foundation, and the ability of the wall to move permanently by translation or rotation should be evaluated to determine whether the MO method can be applied. For the design of major wall structures where the MO method is applicable refinements to the method should be considered. These include investigating the failure plane location to determine whether it is located within the backfill or passes through residual soils that may have significant cohesion, allowing for the increase in dynamic pressures from water in the backfill, and estimating the passive resistance acting on the foundation components to determine the sliding resistance. These refinements are not difficult to calculate. Charts presented in this paper provide a quick method of assessing whether more detailed analysis is required.

REFERENCES

Ambraseys, N. N. and Menu, J. M. 1988. Earthquake–induced Ground Displacements. *Journal of Earthquake Engineering and Structural Dynamics*, Vol 16, 985-006.

Ambraseys, N. and Srbulov M. 1995. Earthquake Induced Displacements of Slopes. *Soil Dynamics and Earthquake Engineering*, Vol 14, 59-71.

Anderson, D. G, Martin G. R, Lam, I. and Wang, J. N. 2008. Seismic Analysis and Design of Retaining Walls, Buried Structures, Slopes and Embankments. *NCHRP Report 611*, Transportation Research Board.

Bray, J. D, Travasarou, T. and Zupan, J. 2010. Seismic Displacement Design of Earth Retaining Structures. *ASCE, Earth Retention Conference*, (ER2010), Washington.

Choudhury, D. 2004. Seismic Passive Resistance at Soil-Wall Interface. Paper No 2746, *13th WCEE*, Vancouver.

Jibson, R. W. 2007. Regression Models for Estimating Coseismic Landslide Displacement. *Engineering Geology*, Vol 91 Issues 2-4, 209-218.

Kramer, S. L. 1996. Geotechnical Earthquake Engineering. Prentice Hall, New Jersey.

Kumar, J. 2001. Dynamic Passive Earth Pressure Coefficients for Sands, *Canadian Geotech. Jour*. Vol 38, 876-881.

Matsuzawa, H, Ishibashi, I. and Kawamura, M. 1983. Dynamic Soil and Water Pressures. *ASCE Jour. Geotech Engineering*. Vol 11(10), 1161-1176.

Mononobe, N. and Matsuo, H. 1929. On the Determination of Earth Pressures During Earthquakes, *Proc World Eng Conf 9*, 177-185.

Morrison, E. E. and Ebling, R. M. 1995. Limit Equilibrium Computation of Dynamic Earth Pressure. *Canadian Geotech. Jour*. Vol 32, 481-487.

Mylonakis, G, Kloukinas, P. and Papantonopoulos, C. 2007. An Alternative to the Mononobe–Okabe Equations for Seismic Earth Pressures. *Soil Dynamics and Earthquake Engineering*, Vol 27, 957-969.

Shukla, S. K. 2013. Generalized Analytical Expression for Dynamic Passive Earth Pressure from c-ϕ Soil Backfills. *International Journal Geotechnical Engineering*, Vol 7(4), 443-446.

Shukla, S. K. 2015. Generalized Analytical Expression for Dynamic Active Thrust from c-ϕ Soil Backfills. *International Journal Geotechnical Engineering*, Vol 9(4), 416-421.

Smith, C. C. and Cubrinovski, M. 2011. Pseudo-static Limit Analysis by Discontinuity Layout Optimization: Application to Seismic analysis of Retaining Walls. *Soil Dynamics & Earthquake Eng.* Vol 31(10), 1311-1323.

Soubra, A. H. 2000. Static and Seismic Passive Earth Pressure Coefficients on Rigid Retaining Structures. *Canadian Geotech Jour*. Vol 37, 463-478.

Subba Rao, K. S. and Choudhury, D. 2005. Seismic Passive Earth Pressure in Soils. *ASCE Jour Geotech Eng.* Vol 113(1), 131-135.

Terzaghi, K, Peck, R. B. and Mesri, G. 1996. Soil Mechanics in Engineering Practice, Wiley & Sons, New York.

Westergaard, H. M. 1933. Water Pressures on Dams during Earthquakes, *Trans. ASCE*, Vol 98.

Wood, J. H. 2008. Design of Retaining Walls for Outward Displacement in Earthquakes. *Proceedings New Zealand Society for Earthquake Engineering Annual Conference*, Wairakei.

Wood, J. H. 2019. Earthquake Design of Flexible Soil-retaining Structures. *Proceedings of the Institution of Civil Engineers – Geotechnical Engineering*, Vol 172, 1 https://doi.org/10.1680/jgeen.17.00192